Earthquakes and Structures, *Vol. 21, No. 6 (2021) 601-612*
https://doi.org/10.12989/eas.2021.21.6.601

Effect of excitation intensity on slope stability assessed by a simplified approach

Aleksandra Korzec*[1] and Robert Jankowski[2a]

[1]*Institute of Hydro-Engineering, Polish Academy of Sciences, ul. Kościerska 7, 80-328 Gdańsk, Poland*
[2]*Faculty of Civil and Environmental Engineering, Gdańsk University of Technology, ul. Narutowicza 11/12, 80-233 Gdańsk, Poland*

(*Received March 19, 2021, Revised September 16, 2021, Accepted September 24, 2021*)

Abstract. The paper concerns the selection of a design accelerograms used for the slope stability assessment under earthquake excitation. The aim is to experimentally verify the Arias Intensity as an indicator of the excitation threat to the slope stability. A simple dynamic system consisting of a rigid block on a rigid inclined plane subjected to horizontal excitation is adopted as a slope model. Strong ground motions recorded during earthquakes are reproduced on a shaking table. The permanent displacement of the block serves as a slope stability indicator. Original research stand allows us to analyse not only the relative displacement but also the acceleration time history of the block. The experiments demonstrate that the Arias Intensity of the accelerogram is a good indicator of excitation threat to the stability of the slope. The numerical analyses conducted using the experimentally verified extended Newmark's method indicate that both the Arias Intensity and the peak velocity of the excitation are good indicators of the impact of dynamic excitation on the dam's stability. The selection can be refined using complementary information, which is the dominant frequency and duration of the strong motion phase of the excitation, respectively.

Keywords: accelerogram; Arias Intensity; dynamics; Newmark's method; shaking table; slope stability

1. Introduction

Natural slopes or man-made earth structures can be affected by ground shaking caused by natural phenomena or induced by human activities (Lowrie 2007). Vibrations induced by mutual movements of rocks along tectonic faults are the most dangerous for massive earthworks. In such cases, additional dynamic loads need to be taken into account in the stability analysis. Earthquake intensity is usually characterized by its magnitude, which is related to the amount of energy released and transmitted by seismic waves during a seismic event (Srbulov 2008). However, this indicator can not be translated directly into forces affecting the structure. The earthquake impact on an endangered object can be forecasted based on the known *ground acceleration* and Newton's relationship between acceleration and inertia force acting on the structure.

A probabilistic approach is recommended to determine a *design acceleration* a_d, but a deterministic approach is also still used (Grünthal 1999, GSHAP, McGuire 2001, Abrahamson 2000, Romeo and Prestininzi 2000). Design acceleration results from the seismicity of the analysed region but also takes into account the importance of the structure, exploitation regime and local ground conditions (Eurocode 8 2004, ICOLD 2016).

The simple slope stability method uses only the peak ground acceleration value. However, more reliable methods take into account the entire time-history of acceleration (Eurocode 8 2004, Gazetas and Dakoulas 1992, Day 2002, Sica *et al*. 2002, Jibson 2001). The *design accelerogram* $A(t)$ is determined based on the accelerogram recorded by seismic station (Aoi *et al*. 2004, Massa *et al*. 2010, Mirek and Lasocki 2001). Signal processing includes filtering, trend elimination (Trifunac 1971, Boore 2005, Boore and Bommer 2005), adjusting the frequency band, and scaling to the design value a_d. Due to the random nature of seismic excitations, the stability of the structure should be assessed based on the maximum response obtained for at least three design accelerograms (Eurocode 8 2004). Bommer and Acevedo (2004), however, suggest that the mean value of the system's responses should be assessed for ten design accelerograms. The records should represent independent earthquakes, so they should not be obtained during the same seismic events and should not be by the same seismic station. However, the question arises how to choose appropriate accelerograms (from among hundreds) which should be used in slope stability analysis?

The selection of earthquake ground motion records should take into account geophysical aspects and an engineering measure of ground motion, as well as, the characteristics of the designed structure (Haselton 2009, Katsanos *et al*. 2010). First of all, the predicted magnitude range of earthquakes and the most probable epicentre distances are used for the initial selection of signals. Second, it is recommended to select accelerograms that were recorded during earthquakes with the same fault mechanism as predicted for the site. However, due to the lack of a confirmed clear influence of the mechanism on the reason of vibrations, this criterion is sometimes omitted (Katsanos *et al*. 2010). Moreover, local geology influences

*Corresponding author, Ph.D.
E-mail: a.korzec@ibwpan.gda.pl
[a]Professor

ISSN: 2092-7614 (Print), 2092-7622 (Online)

the surface ground motion, so the local soil profile should be used as a criterion. Next, the accelerogram parameters, such as its *peak value*, *strong phase duration* or *intensity*, are analysed. Finally, it is recommended to check the compliance of the average response spectrum of the oscillator subjected to selected excitations with the spectrum given by code provisions or computed directly through a probabilistic seismic hazard assessment (Eurocode 8 2004, Czerwionka and Tatara 2007, Jayaram *et al*. 2011, Kaveh and Mahdavi 2017).

This article aims to verify experimentally the relationship between excitation energy and its influence on slope stability assessed by a simplified approach. The experiments were designed to reflect the slope analogue proposed by Newmark in 1965, which is the most commonly used approach for the preliminary assessment of global slope stability under seismic loading. Newmark's concept of *sliding block* permits a temporal loss of stability, expressed by a limit equilibrium between driving and resisting forces along a potential slip plane. The method assesses the permanent displacement of the slope accumulated during all phases of relative motion. In this paper, the experimentally verified extended Newmark's method is incorporated. It should be underlined that the method is suitable for soils that are not prone to liquefaction. The study takes into account horizontal excitations only, as they are the main driving dynamic loading.

The article structure is as follows. Firstly, in Section 2, the accelerogram parameters used in the paper are defined. The extended Newmark's method is briefly described in Section 3. Further, in Section 4, the research stand, the excitation used and the methodology of data analysis are presented. Then, the results of the experiments are presented and discussed. The validation of the extended Newmark's method in the case of real-life excitations is presented in Section 5. Further, in Section 6, the numerical simulation showing the usefulness of accelerogram parameters as an indicator of the excitation impact on slope stability is discussed. Conclusions are given in Section 7.

2. Accelerogram parameters

The acceleration time-history can be characterised by its absolute maximum value, also called the *peak ground acceleration PGA*, Fig. 1. The first preselection takes into account the consistency of the design acceleration a_d and the recorded *PGA* value. The scaling factor of *PGA* should not be less than 0.5 or more than 2 to avoid scaling the noise (Bommer and Acevedo 2004). Because all accelerograms need to be scaled to the same value a_d, another parameter should be utilized as an indicator of the most dangerous excitation for the structure. The Fourier transform of the accelerogram enables us to identify the dominant frequency f_I, characterised by the highest amplitude, or the range of dominant frequencies, Fig. 2. The dominant frequencies of strong-motion records are usually in the range of 2÷3 Hz, whereas rockburst induced ground motion records are characterised by higher dominant frequencies, often in the range of 3÷5 Hz (Burkacki and Jankowski 2019, Burkacki *et al*. 2020). When assessing stability based on the dynamic response of structure (e.g., displacement) f_I is an important indicator in the selection of the design accelerogram. An accelerogram with f_I which is as close as possible to the natural frequency of the structure, should be selected. However, when the stability assessment is carried out using a *simplified method*, such as Newmark's method (1965), which assumes the stiffness of the potential sliding wedge, the parameter f_I alone is unlikely to be useful. However, comparing the amplitude spectra $|F_A|$ could be helpful due to its relationship to a *peak ground velocity* (*PGV*) and energy of the motion. The lower the frequencies of the relevant component waves, the higher the *PGV* and energy. To correctly determine the *PGV* the recorded accelerogram has to be pre-processed to eliminate noise and trends (Boore and Bommer 2005, Yang *et al.* 2006).

The energy of seismic waves is most often expressed by the *Arias Intensity* (I_a) (Arias 1970). It expresses normalized total energy absorbed by a simple un-damped oscillator excited by a set of mono-harmonic waves (of an evenly discretized frequency domain of excitation). For a single component of motion, it is given by Eq. (1)

$$I_a = \frac{\pi}{2g}\int_0^{t_c} A(t)^2 dt, \tag{1}$$

where g denotes acceleration due to gravity, $A(t)$ ground acceleration time-history, and t_c total duration of an accelerogram. The unit of I_a is m/s. Accelerograms can also be classified according to their duration, in particular, the duration of a strong shaking, called latter a *strong motion phase*. This phase can be defined in various ways. One of them uses the so-called *bracketed duration* t_B, proposed by

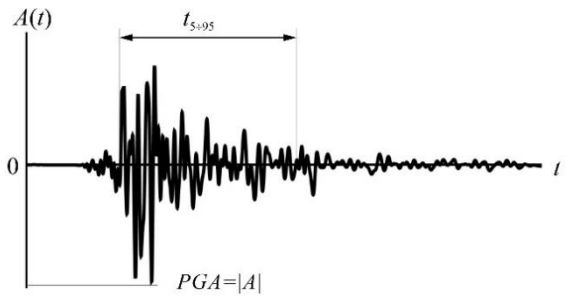

Fig. 1 Accelerogram $A(t)$ and its parameters: peak ground acceleration *PGA* and duration of strong shaking phase $t_{5\div95}$

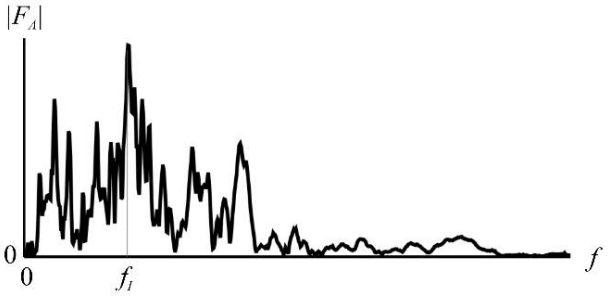

Fig. 2 Amplitude spectrum of accelerogram $|F_A|(f)$ and its dominant frequency f_I

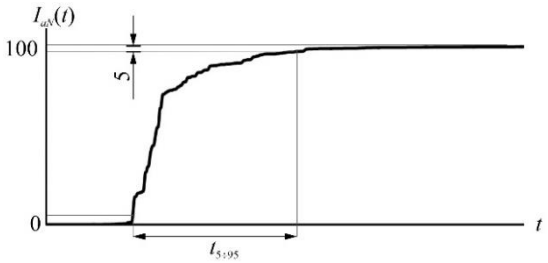

Fig. 3 Plot of normalized Arias Intensity IaN(t) and definition of Trifunac and Brady's (1975) duration of strong motion t5÷95

Bolton (1969), and it is defined on basis of the first and the last exceedance of an acceleration threshold. The threshold values for natural earthquakes are assumed to be 0.05 g (Abrahamson 2000). Another definition is based on the determination of the increase in the *normalized Arias Intensity* $I_{aN}(t)$ from 5% to 95%, Fig. 3. This measure, denoted here as $t_{5\div95}$, was proposed by Trifunac and Brady (1975) and it is used very often.

The present article is focused on the accelerogram parameters and their impact on slope stability. The question is which of the parameters should be used as a criterion for selecting the excitation of critical potential effects for the designed structure (Neethu *et al*. 2017, Pejovic *et al*. 2017, Tsinidis *et al*. 2020). The strong-phase duration would be appropriate for fatigue-prone structures or cases of soils susceptible to liquefaction when the number of loading cycles is a crucial parameter. However, in the case of brittle structures, the maximum additional force would be of more importance. In the case of buildings subjected to mining tremors, *PGV* was identified as a good criterion (Zembaty 2004). Sarma and Kourkoulis (2004) stated that to predict the sliding displacements accurately enough 'some idea of the average duration and the number of pulses in acceleration records is necessary' together with the peak acceleration and peak velocity. Concerning global slope stability, the Arias Intensity is the most useful (Jibson 1994, 2007, Kramer 1996, Lanzo *et al*. 2015, Romeo 2000, Travasarou 2003, Chousianitis *et al*. 2014). However, Garini *et al*. (2011) demonstrated that the Arias Intensity cannot alone could not be a reliable predictor of slip.

3. Extended Newmark's method

The sliding block concept proposed by Newmark (1965) is widely used for the stability assessment of slopes. In the present paper, the extended Newmark's method is used (Korzec 2016, Korzec and Jankowski 2021). A simple dynamic system that consists of a rigid block resting on an α inclined plane serves as a slope model, Fig. 4. The horizontal excitation $\mathbf{A_x}(t)$ of the rigid base induces the inertia force $\mathbf{F_{dx}}(t)$ acting on the block. A local coordinate system tangent and normal to the slip plane (s, n) is used to analyse the dynamic stability of the block. The mass of the block is assumed to ensure that the block will not be lifted off the ground. However, the block can move up and down along the slip plane. The critical acceleration value that can be transferred to the block is determined from an equilibrium between a sliding $\mathbf{T}(t)$ and a resisting $\mathbf{S}(t)$ forces. According to Coulomb's law, the resisting force results from friction between two rigid bodies, described by friction coefficient μ. It is worth noting that, in contrast to the original Newmark's method, the extended Newmark's method assumes an impact of the dynamic force on the resisting force. Fig. 4 shows the balance of forces at a specific moment when the dynamic horizontal load decreases the resisting force. Whenever the excitation component tangent to the α inclined slip plane A_s reaches the critical acceleration a_c (given by Eqs. (2)-(3) the relative movement of the block is initiated.

$$A_s(t) < -g(\mu cos\alpha - sin\alpha) - \mu A_x(t) sin\alpha = a_c^-, \quad (2)$$

$$A_s(t) > g(\mu cos\alpha + sin\alpha) - \mu A_x(t) sin\alpha = a_c^+. \quad (3)$$

The motion of the block is obtained by a method proposed by Sawicki and Chybicki (2005). First, the second-order differential equation is substituted by two first-order differential equations (velocity and displacement derivatives). Then, they are approximated by the central finite difference method. The time step of 0.001 s is used. Knowing the displacement time-history of the foundation and the block, the relative displacement time-history of the block $u_{rel}(t)$ is determined. Next, the permanent displacement D of the block accumulated during shaking is determined and it serves as a slope stability indicator. The determined D value is then compared with the assumed

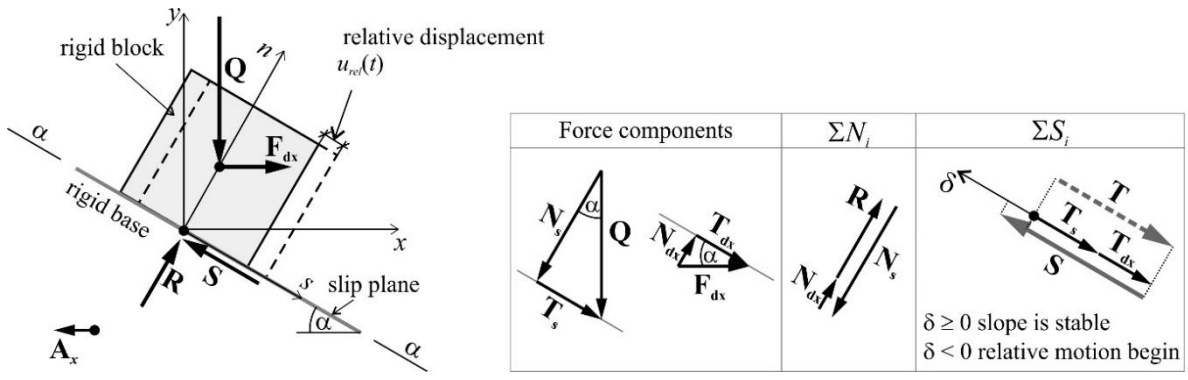

Fig. 4 Concept of extended Newmark's method for specific moment when dynamic horizontal excitation $\mathbf{A_x}$ reduces resisting force **S** due to reduction of resultant normal force **R** (**Q**-own weight force; **N**-normal force, **T**-sliding force, $\mathbf{X_s}$-static component of **X**, $\mathbf{X_{dx}}$-dynamic component of **X** induced by horizontal inertia force $\mathbf{F_{dx}}$)

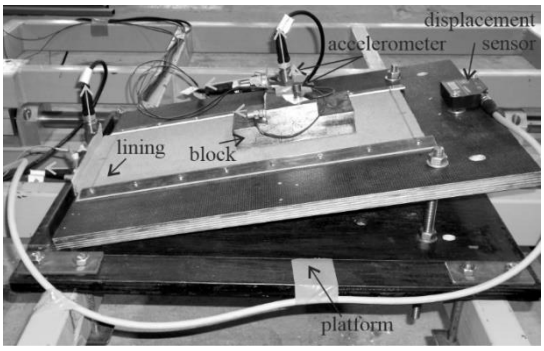

Fig. 5 Slope model with sensors

critical value D_c and a conclusion is made regarding the stability assessment. The critical value D_c concerns not only the safety of the slope itself but also, the safety of associated infrastructure, such as pipelines or spillways.

4. Experiments

4.1 Experimental stand

The experimental stand consists of a *slope model*, a *dynamic load generator* and a *measuring system*. The slope model reflects the assumptions of the theoretical model. A platform with adjustable inclination serves as an inclined slip plane, while a steel block with a rectangle base of 8×16 cm and a mass of 3.815 kg models a potential sliding mass, Fig. 5. The friction properties of the interface between the block and the platform are determined by different materials covering the two planes. The results presented in the paper were obtained for a sliding plane inclination of around 10° and an interface made from a sand paper (grain size 100) and fibreboard.

The frictional properties of the interface were established in a separate test by pulling the block along a horizontal plane using a screw actuator. Sensors and acquisition system used are produced by Hottinger Baldwin Messtechnik GmbH (HBM). S-shaped S2M force transducer with a nominal measuring range of 100 N and an accuracy of 0.02 N was used to measure the pulling force S_p. An inductive displacement transducer WA-T with a measuring range of 10 mm and an accuracy of 0.1 mm was installed to measure the block displacement u_s. SPIDER 8 data acquisition system with the Catman software was employed to record data with a frequency of 100 Hz. Fig. 6 shows the results of the five tests performed. For each test, the friction coefficient of the investigated interface was calculated as the ratio of the pulling force S_p and the normal force resulting from the mass of the block. The static friction coefficient μ_s was determined based on the maximum value of S_p before the block movement (specifically for u_s less than 0.5 mm). The kinetic friction coefficient μ_k was calculated based on the pulling forces recorded during the relative motion of the block (0.5 mm to 2.0 mm). The analysed interface is characterized by the average static friction coefficient μ_s of 0.84 with the coefficient of variation of 3.6% and by the average kinetic

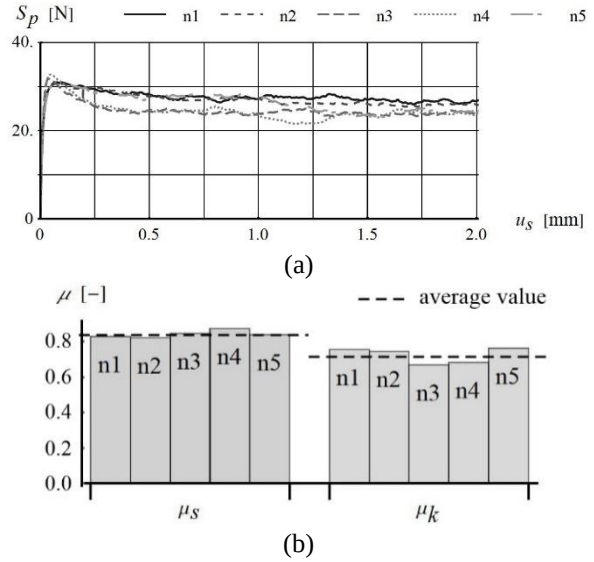

Fig. 6 Friction characteristics of interface applied. (a) Changes of pulling force S_p with increasing relative displacement of block along horizontal slip plane u_s. (b) Static μ_s and kinetic μ_k friction coefficients obtained in five tests

friction coefficient μ_k equal to 0.71 ($0.84\mu_s$) with the coefficient of variation 5.9%. The platform is rigidly attached to a uniaxial shaking table. The horizontal motion of the shaking table is generated by a Parker ET125 electric actuator controlled by a Velleman PCSGU250 PC function generator (for more details see Falborski and Jankowski 2017, 2018, Jaroszewicz *et al*. 2016). The motion is defined by the velocity time-history with a peak value of 1 m/s and a scaling factor κ. Thus, it is possible to generate strong motions recorded during earthquakes.

The platform and the block are equipped with piezoelectric accelerometers produced by VibraSens and PCB Piezotronic. The measuring range of the VibraSens 101.01-9 type accelerometer is ±10 g, while that of the PCB type 352C33 is ±50 g. Both types of sensors have the same voltage measurement range (±5 V). The small mass of the PCB accelerators, which is only 5.8 g, and their flexible wiring preclude any impact on the dynamic behaviour of the block. The average noise amplitudes, measured before and after the experiments, were equal to 0.008 m/s^2 and 0.037 m/s^2, respectively, for the VS sensors and the PCB accelerometer types. A Micro-Epsilon laser displacement sensor was mounted to the platform so as to measure the block displacement. The measuring range of the adopted sensor is 200 mm, and the average amplitude of noise recorded during preliminary tests was 47 μm. Voltage signals from the sensors were processed by an ALITEC VIMEA VE 16BCA measurement system with an accuracy of ±0.1V±0.5% and managed by the VIMEA SVDA v.1.1 software. The data acquisition frequency was set to 1024 Hz.

4.2 Excitations applied

Strong ground motions recorded during the Kobe

Table 1 Characteristics of selected earthquakes

Name	Country	Year	Magnitude M_w [-]	Seismic station	Distance [km]	Waveform
Kobe	Japan	1995	6.8	Kakogawa	3.4	RSN1107_KOBE_KAK
Northridge	USA	1994	6.7	Rinaldi	7.5	RSN987_NORTHR_CEN155
San Fernando	USA	1971	6.6	San Fernando	7.0	RSN77_SFERN_PUL254

Table 2 Characteristics of generated excitations (filtered with frequency cut-offs of 0.1 Hz and 20 Hz)

Excitation no.	pA [m/s^2]	I_a [m/s]	pV [m/s]	f_1 [Hz]	$t_{5\div95}$ [s]
#1	7.79	**8.94**	**0.94**	**1.44**	**9.29** (4.84÷14.13)
#2	9.78	3.14	0.36	4.39	8.64 (8.34÷16.98)
#3	9.56	7.20	0.44	2.32	7.23 (5.04÷12.27)

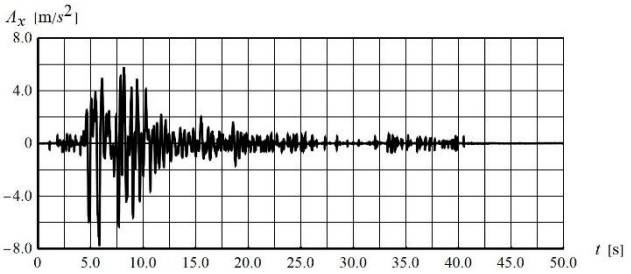

Fig. 7 Accelerogram #1 obtained (filtered with frequency cut-off of 0.1 Hz and 20 Hz)

earthquake in 1995, the Northridge earthquake in 1994 and the San Fernando earthquake in 1971 were selected for the tests. These seismic events had similar moment magnitude M_w, Table 1. In all three cases, the seismic stations were located at a close distance to the earthquake epicentres. The horizontal acceleration time-histories were taken from the NGA database developed by the *Pacific Earthquake Engineering Research Center PEER* (Chiou *et al*. 2008).

As mentioned in the previous section, the actuator motion was defined in the software by velocity time-history scaled to 1 m/s and the scaling factor κ. The velocity time-histories were obtained by numerical integration. Scaling factors κ were established based on preliminary tests and the observed value of permanent displacements of the block.

Due to scaling, the obtained accelerograms do not reflect the course of earth movements recorded by seismic stations. Therefore, they were marked with subsequent numbers (#1, #2, #3) instead of using earthquakes name. The horizontal accelerograms recorded on the platform during experiments are shown in Figs. 7-9. Fig. 10 compares the amplitude spectra of the accelerograms obtained. The parameters characterizing the generated excitations are presented in Table 2. To distinguish the parameters of the real-life accelerograms from the generated ones, the symbol of the peak acceleration and velocity value of the accelerograms obtained are denoted by pA and pV. The generated excitations differ in energy, which is fundamental for the conducted experiments. Fig. 11 compares the Arias Intensity time-histories $I_a(t)$ and the I_a values are given in Table 2. The excitation #1 has the

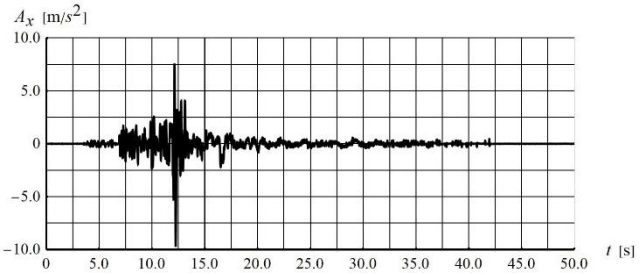

Fig. 8 Accelerogram #2 obtained (filtered with frequency cut-off of 0.1 Hz and 20 Hz)

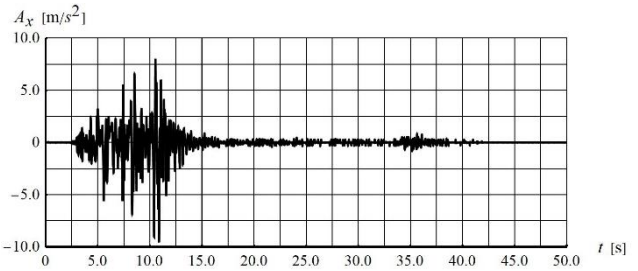

Fig. 9 Accelerogram #3 obtained (filtered with frequency cut-off of 0.1 Hz and 20 Hz)

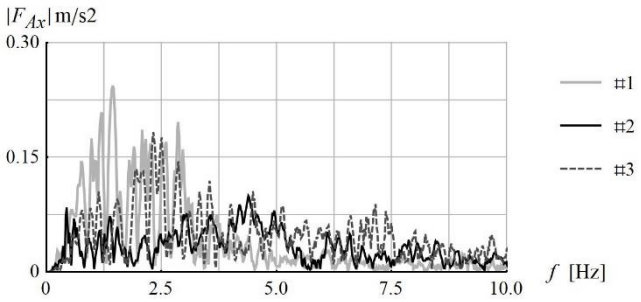

Fig. 10 Comparison of amplitude spectra $|F_{Ax}|(f)$ of excitations obtained (filtered with frequency cut-offs of 0.1 Hz and 20 Hz)

highest intensity of 8.94, although it has the smallest pA value. The I_a of the *#2* excitation is twice as high as that of the *#3* excitation, although the pA values differ by only 1.7%. The strong-phase duration $t_{5\div95}$ of these excitations ranges from 7.23 s to 9.29 s.

4.3 Data analysed

The displacement time-histories of the block $u_{rel}(t)$ relative to the platform and the time-histories of platform $A_s(t)$ and block $a_s(t)$ acceleration component tangent to the slip plane were analysed. First, the permanent displacement of the block was determined from the last recorded value of the relative displacement of the block $u_{rel}(t)$. Second, the number of *phases of relative motion* was identified and

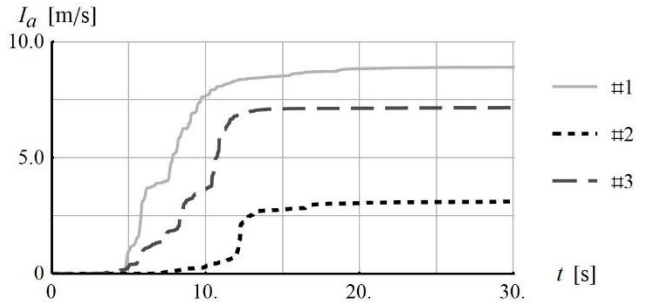

Fig. 11 Comparison of Arias Intensity time-histories I_a(t) of excitations obtained

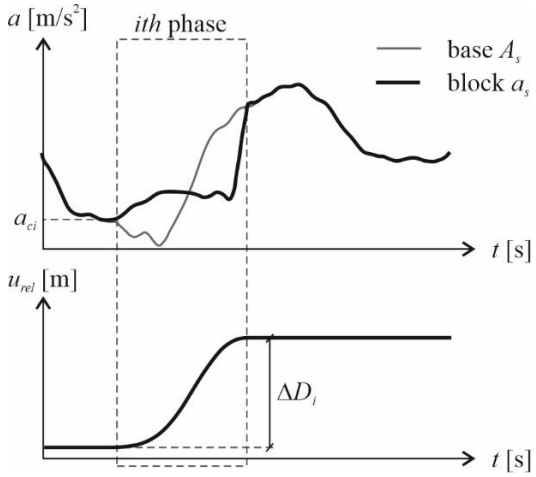

Fig. 12 Determination of relative phase motion and critical acceleration a_c (ΔD_i-permanent displacement increments during ith phase)

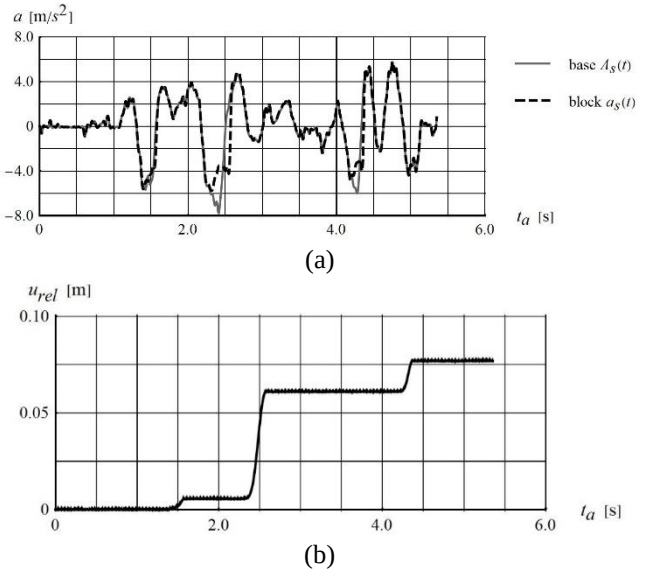

Fig. 13 Time-histories of (a) platform $A_s(t)$ and block $a_s(t)$ acceleration component tangent to slip plane, (b) relative displacement of block induced by #1 excitation

Table 3 Critical accelerations and permanent displacement increments in successive phases recorded during tests

Name	a^-_{ci} [m/s^2]			ΔD_i [mm]			D [mm]
	1	2	3	1	2	3	
Kobe 1995	-5.40	-5.19	-4.93	8.08	55.51	13.70	77.29
Northridge 1994	-5.09	-4.95	UN	0.72	17.36	UN	18.08
San Fernando 1971	-5.11	-4.88	UN	3.63	10.12	UN	14.95

permanent displacement increments ΔD_i accumulated during each of them were determined. The *phase of relative motion* means the time interval when the absolute value of the block acceleration becomes smaller than the absolute value of the platform acceleration and, at the same time, the block displacement relative to the platform is initiated, Fig. 12. The time of the block movement initiation is determined from the $u_{rel}(t)$ derivative. The *critical acceleration* a_c was determined from the block acceleration at that time instance. Knowledge of this parameter allows us to confirm the repeatability of friction properties in successive experiments. These data also provide an insight into the variability of the a_c due to material variability, which influences the obtained permanent displacement of the block.

The accelerograms were filtered using the 8th order bandpass Butterworth filter with cut-off frequencies of 0.1 Hz and 20 Hz. The lower limit of the frequency resulted from the analysis of noise registered by accelerometers. In contrast, the upper limit was based on the assumption that waves with a frequency higher than 20 Hz would not affect block behaviour. For the sake of clarity, only results for selected periods are presented in this paper using the local time t_a. The time interval limits are defined by the percentage representation of the *Arias Intensity*.

4.4 Experimental results

First, the results obtained for the *#1* excitation are presented. The time interval of data presented here covers the excitation I_a range from 5% to 15%. Fig. 13(a) shows the recorded time-series of the block $a_s(t)$ and platform $A_s(t)$ acceleration components tangent to the slip plane. The displacement time-history of the block relative to the platform $u_{rel}(t)$ is presented in Fig. 13(b). Three phases of the relative motion of the block are identified, which are marked with consecutive numbers, Table 3. The maximum absolute value of acceleration towards the top of the slope transmitted to the block, called critical acceleration a^-_c, described by Eq. (2), is -5.4 m/s^2. The variability of the friction properties of the interface also causes a noticeable difference in the a_c value between phases of relative motion, Table 3. The maximum a^-_c difference is 8.7%. The permanent displacement of block D accumulated during that excitation is equal to 77 mm. The successive increments ΔD_i are given in Table 3.

In the case of *#2* excitation, the permanent displacement of 18 mm is accumulated during two phases of relative motion, Fig. 14. However, most of them (92%) are accumulated during the second phase. The time interval of motion presented here covers an increase in the Arias Intensity of the excitation from 21% to 33%. The critical acceleration a^-_c is estimated at 5.0 m/s^2.

In the case of the #3 excitation, the block is displaced permanently by 15 mm, Fig. 15(b). The time interval of the

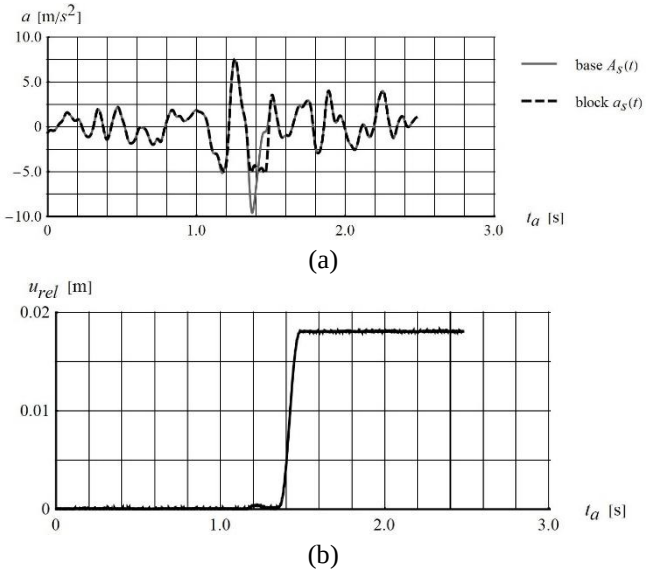

Fig. 14 Time-history of (a) platform $A_s(t)$ and block $a_s(t)$ acceleration component tangent to slip plane, (b) relative displacement of block induced by #2 excitation

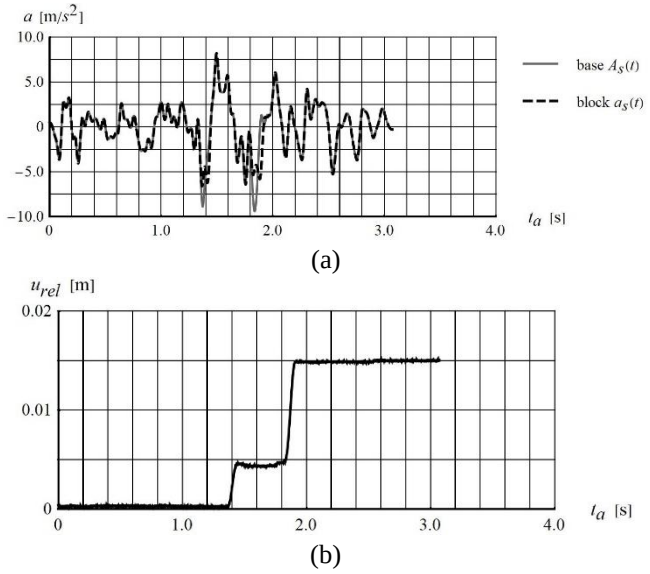

Fig. 15 Time-history of (a) platform $A_s(t)$ and block $a_s(t)$ acceleration component tangent to slip plane, (b) relative displacement of block induced by #3 excitation

presented excitation covers an increase in the Arias Intensity from 32.0% to 37.5%, Fig. 15. Two phases of relative motion are identified. The acceleration that initiates the relative movement of the block differs between those phases. The critical acceleration values are determined equal to -5.1 m/s^2 and -4.9 m/s^2.

4.5 Discussion of experimental results

The paper aims to experimentally prove the relationship between the excitation intensity described by Arias Intensity I_a, and slope stability expressed by permanent displacement *D*. Two of the excitations analysed, i.e., #2 and #3, had *pA* values approximately 23% higher than the *pA* value of the #1 excitation but produced an 80% lower permanent displacement. A comparison of the I_a of the generated excitations indicates that it is a good measure of the impact of excitations on the slope stability. Excitation with the highest intensity I_a induced the greatest permanent displacement *D*. This comparison also indicates that *pA* is not a reliable parameter in assessing the impact of excitation on the block stability.

It is worth noting that during the #2 and #3 excitations the block was displaced by almost the same distance although the I_a of the #3 excitation is twice as larger as that of the #2 excitation. This is because the permanent displacement in both cases was accumulated during two cycles. However, in the case of a weaker interface, the permanent displacement would be far much greater for the #3 excitation than for the #2 excitation, which is characterised by a single acceleration peak. Auxiliary research results obtained for interface characterised by a_c of about 4.0 m/s^2 confirmed this presupposition. The block was displaced permanently by 48 mm during the #3 excitation and by 33.2 mm during the #2 excitation. Therefore, the Arias Intensity still seems to be a good measure of the impact of excitation on global slope stability. Bearing the above in mind, it is also worth assessing the shape of the accelerogram, not just I_a value.

Furthermore, it is worth noting that permanent displacement was accumulated over a short time interval. In the cases analysed, the Arias Intensity of excitations increased by a maximum of about 10% during the period of permanent displacement accumulation. Presumably, a significant difference in the duration of strong motion phase may lower the accuracy of the Arias Intensity criterion.

In the cases analysed here, the highest peak velocity of excitation indicates well the signal most dangerous for the slope stability.

The recorded critical accelerations confirmed the similarity of the friction properties of the interface in the tests performed. The average critical acceleration of seven a_{ci} determined in all tests was 5.08 m/s^2 with a coefficient of variation of 3.3%. Hence, the a_c variability of friction properties, which is natural and unavoidable, is similar to that obtained in pull tests. When analysing a single test, a downward trend in a_{ci} is noticeable, which may indicate a degradation of friction properties in every successive phase of relative motion. The maximum difference was 8.7%. However, the pull test showed degradation of friction properties for that type of contact after 10 cycles. Thus, the cause of the decrease in a_c is not clear.

The above-mentioned variability of a_c affects permanent displacement accumulated during shaking. This knowledge helps to understand possible discrepancies between the results of a numerical simulation carried out for a constant value of the friction coefficient and the results of experiments.

5. Model validation for strong motion records

The extended Newmark's numerical model, described in Section 3, was previously validated for mono- and

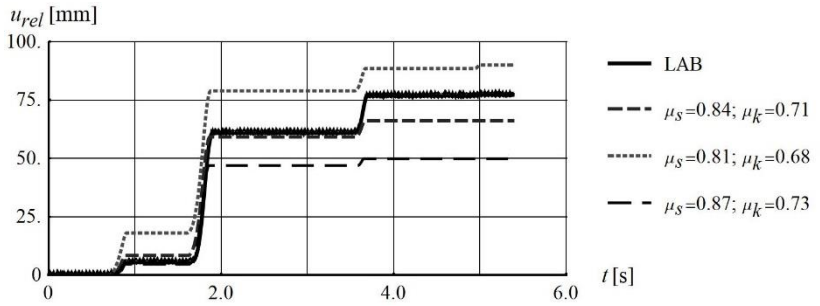

Fig. 16 Comparison of recorded (LAB) time-histories of relative block displacement $u_{rel}(t)$ and those calculated by extended Newmark's method for lower, average and upper estimate of friction coefficients (platform inclined at 9.93° subjected to #1 excitation)

Table 4 Comparison of permanent block displacements and their increments obtained by numerical simulations for different values of friction coefficient with displacements measured (LAB) during *#1* excitation test

Test	Method	μ_s [-]	μ_k [-]	ΔD_i [mm]				D [mm]	Δ_D [%]
				1	2	3	4		
LAB	**recorded**	–	–	**8.08**	**55.51**	**13.70**	–	**77.29**	Reference
1	extended Newmark's	0.84	0.71	8.39	50.79	6.94	–	**66.12**	**-14.5**
2	extended Newmark's	0.81	0.68	18.04	60.87	9.55	1.51	89.98	16.4
3	extended Newmark's	0.87	0.83	4.60	42.30	2.96	–	49.87	-35.5
4	original Newmark's	0.81	–	–	7.09	–	–	7.09	-90.8

* – values of the friction coefficient selected within the range of values determined in the laboratory for the best compliance with the measurement results.

bidirectional cyclic excitations (Korzec and Jankowski 2018, Korzec and Jankowski 2021). The present experimental results are also used for validation of the model in the case of strong-motion records. Only the results obtained for the #1 excitation are presented. First, the calculated permanent displacement D as well as the increments of permanent displacement in successive phases of relative motion ΔD_i are compared with the measured values. The number and timing of successive phases of relative motion are then compared. Finally, the calculated time-history of the block acceleration component tangent to the slip plane $a_s(t)$ is checked for compliance with the recorded one.

The permanent displacement of the block is well predicted by the extended Newmark's method by assuming in the simulations the average value of the friction coefficient (μ_s=0.84 and μ_k=0.71) obtained from the pull tests, Fig. 16. The calculated value of 66.1 mm is lower than the measured one (by 14.5%), Table 4. The increments of the permanent displacement of the block in the successive phases differ by 3.8%, 8.5% and 49.3% from the recorded values. Fig. 16 and Table 4 compare also the numerical results obtained for the upper and lower bound of the friction properties (the mean value plus/minus one standard deviation). The results show that the dynamic system considered here is very sensitive to changes in friction parameters. The error in determining the permanent displacement accumulated during shaking, calculated in relation to the measured values, for the upper bound of the friction properties reaches as much as 35.5%. It is a large number, bearing in mind that the variation coefficient of μ_s in the analysed case is just 3.6%. Greater uncertainty of D estimation results from different amplitudes in individual phases of relative motion, and thus from their different duration. It may even happen that a different number of phases will appear for the upper and lower estimate of the friction coefficient.

Fig. 17 compares the recorded and calculated time-histories of the acceleration component tangent to the slip plane. The block acceleration time-history obtained by the extended Newmark's method follows the experimental results. Specifically, the reproduction of a sharp drop in acceleration after the initiation of the phase of relative motion deserves attention. Such good compliance with the experimental results is achieved by incorporating in the numerical model the reduction in friction properties and the impact of the normal component of the resultant force on the resisting force. At the same time, the assumption of the original Newmark's method regarding the constant acceleration of the block during the phase of relative motion must be rejected.

It is also worth noting that the maximum value of permanent displacement obtained by the original Newmark's method, assuming the lowest estimate of the coefficient of friction (μ_s=0.81), is equal to 7.1 mm, which is around 9% lower than the measured value, Table 4. Moreover, the permanent displacement is accumulated only in one phase, Fig. 18.

6. Numerical experiments

The extended Newmark's method, described in Section 3 and experimentally verified in Section 5, is now used to

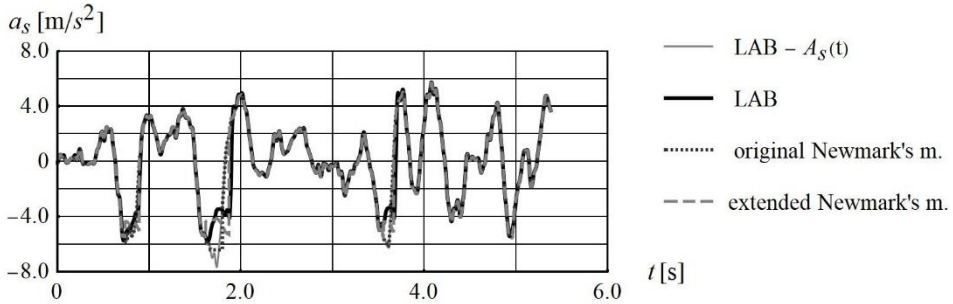

Fig. 17 Comparison of recorded time-histories of block acceleration tangent to the slip plane (LAB) and those calculated by original and extended Newmark's methods (platform inclined at 9.93° subjected to #1 excitation, the average estimate of friction coefficient: μ_s=0.84 and μ_k=0.71)

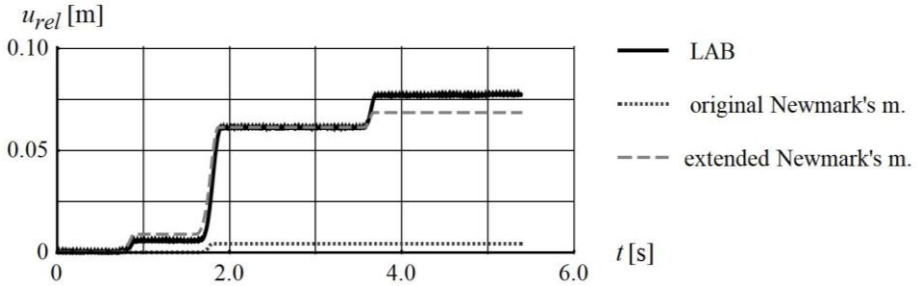

Fig. 18 Comparison of recorded time-histories of relative block displacement (LAB) and those calculated by original and extended Newmark's methods (parameters are given in Fig. 17)

examine accelerogram parameters as an indicator of the most dangerous accelerogram for the slope stability. It is assumed that the analysed slope is located in an area of moderate seismicity, and the predicted acceleration value is 0.4*g*. The inclination of the sliding plane is assumed to be 20° and it is characterized by the static friction coefficient of 0.4.

6.1 Excitation

Three groups of accelerograms were downloaded from the *European strong-motion database* that stores the records of earthquakes that occurred in Europe between 1978 and 2008. The indicated groups differ in the average probable earthquake's moment magnitude M_w that could cause the above-mentioned accelerations: M_w=3; M_w=4; M_w=5. In accordance with the recommendations given by Bommer and Acevedo (2004) concerning the criteria for selecting the design accelerograms, the M_w accuracy of 0.5 was assumed. Additionally, the condition was adopted regarding the peak horizontal acceleration. It should be not greater than twice the predicted acceleration value and not less than half of this value (Bommer and Acevedo 2004). A total of 140 corrected noise-free accelerograms were collected, therefore, no additional processing beyond scaling was applied (ESD 2015, Ambraseys *et al*. 2004).

The calculations were performed according to the scheme presented in Fig. 19. Two mutually perpendicular horizontal components were considered in the calculation. The accelerogram with the higher peak value denoted $H(t)$ was scaled to the design value a_d, while the second one $T(t)$ according to the recorded ratio of peaks of both horizontal components k_{TH}. Due to the expected asymmetry of ground

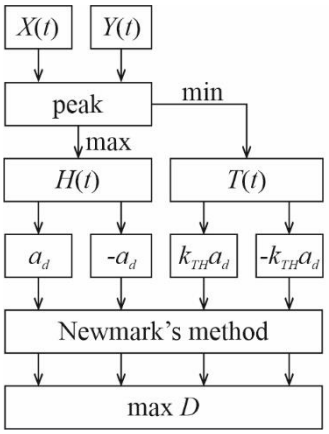

Fig. 19 Load variants analysed

vibrations, the calculations were performed twice for each of the signals. The average ratio of the Arias Intensity in both directions for the analysed set of accelerogram is 0.87 with a coefficient of variation of 13%. The minimum value of this ratio is 0.45. The average ratio of the peak velocity in both directions is 0.76 with a coefficient of variation of 20%. The parameters of horizontal components that induced maximum permanent displacement D was calculated and forwarded for further analysis.

6.2 Simulations results

Figs. 20-22 show the relationship between the permanent displacement accumulated during excitation and parameters of dynamic excitation: Arias Intensity, peak velocity and dominant frequency. Data divided according to the earthquake's magnitude criterion does not create

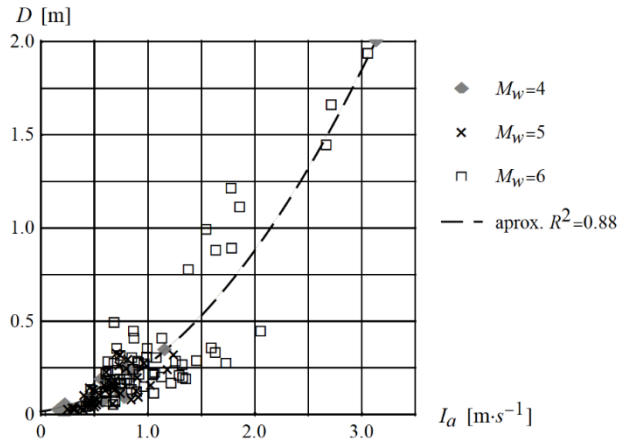

Fig. 20 Dependence of permanent displacements on intensity of excitation (M_w-earthquake's moment magnitude)

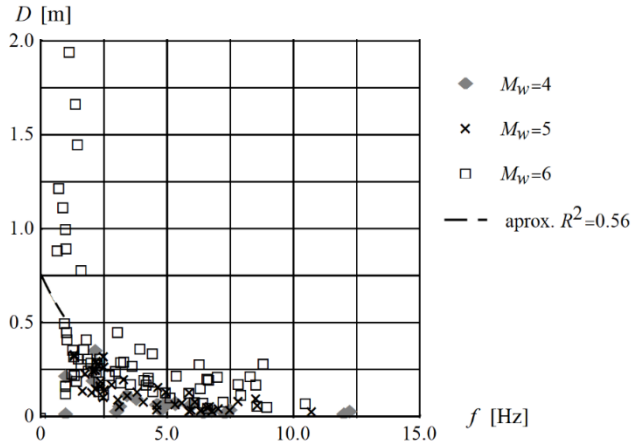

Fig. 22 Dependence of permanent displacements on dominant frequency of excitation (M_w-earthquake's moment magnitude)

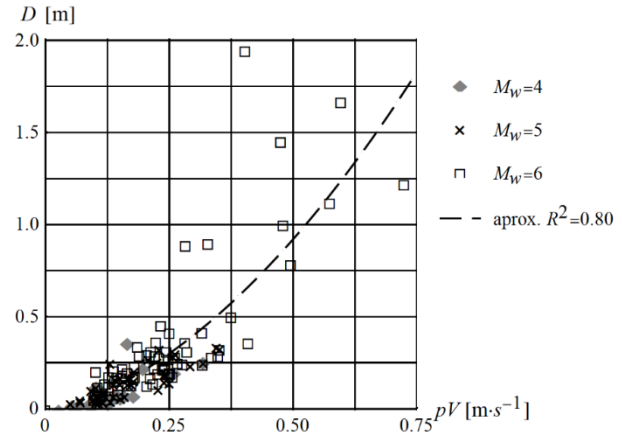

Fig. 21 Dependence of permanent displacements on peak velocity of excitation (M_w-earthquake's moment magnitude)

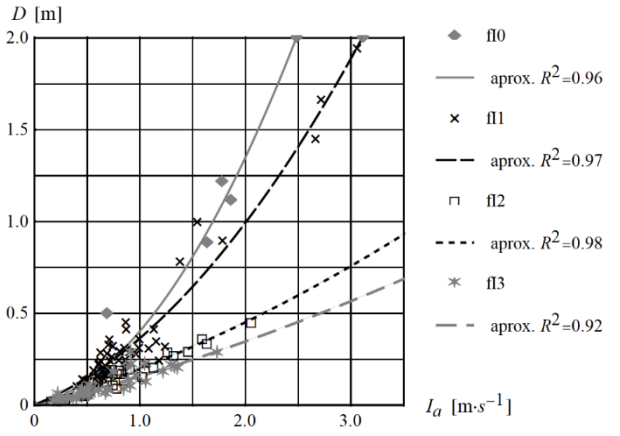

Fig. 23 Dependence of permanent displacements D on Arias Intensity of excitation I_a categorized by dominant frequency of excitation f_I marked as fI0; fI1; fI2; fI3

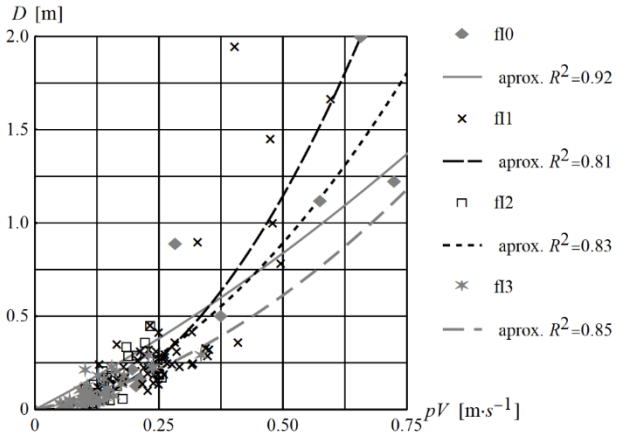

Fig. 24 Dependence of permanent displacements D on peak velocity of excitation pV categorized by duration of strong motion phase of excitation $t_{5\div95}$ marked as T0,T1,T2,T3

convincing trends. Therefore, for each parameter, the trend was obtained based on all of the excitation regardless of the earthquake's magnitude. Nonlinear approximation of the data is used. The obtained coefficients of determination R^2 are equal to 0.88, 0.80, 0.56 for I_a, pV and f_I respectively. The conducted analyses indicate that the Arias Intensity is a good indicator of the impact of dynamic excitation on the slope stability. However, still, some results are confusing. For example, for the excitation characterised by Arias Intensity of 1.75 m/s, two very different permanent displacements can be expected, 0.3 m or 1 m, Fig. 20. The peak velocity of excitation also characterizes well the impact of the excitation on the slope stability. The dominant frequency can be a helpful indicator only when choosing between excitations of the same Arias intensity.

Further research was carried out to refine the I_a and pV selections. Firstly, all the results were divided into four categories according to the duration of strong motion phase (T0: up to 2 s; T1: 2-5 s; T2: 5-10 s, T3: over 10 s). Secondly, four frequency categories were employed (fI0: up to 1 Hz; fI1: 1÷3 Hz; fI2: 3÷5 Hz, fI3: over 5 Hz). In the case of Arias Intensity, the frequency category effectively separates the data and indicate the excitation inducing the highest permanent displacement, Fig. 23. R^2 for each subset of data, besides fI3, is not less than 0.96. The lower the f_I value, the greater the expected impact of the excitation on the slope stability. On the other hand, it seems counter-intuitive that adding the duration of the strong movement phase does not increase the accuracy of this criterion. The

selection made by the peak velocity criterion can be refined using the duration of the strong motion phase of excitation. The higher the $t_{5\div95}$ value, the greater the expected impact of the excitation on the slope stability, Fig. 24. R^2 for each subset of data, besides T3, is not less than 0.94.

7. Conclusions

The shaking table experimental tests were conducted using a simple slope model. Three excitations were generated to reproduce the complexity of accelerograms recorded during earthquakes. The friction properties of the interface between the block and the platform with adjustable inclination were determined in a pull test. The similarity of the friction properties of the interface in the tests was also confirmed by analysing the critical accelerations.

The experimental results show that the *Arias Intensity* is a good indicator of the excitation threat to the slope stability. The higher the excitation intensity, the higher the permanent displacement of the slope. However, the *strong-phase duration of the signals* must be similar. Moreover, while selecting the accelerograms, their shape should also be checked so as to avoid the records with a single peak. Alternatively, the variation of the *Arias Intensity* in time can be analysed. If possible, an accelerogram with a very steep and very flat *normalized Arias intensity* curve should be avoided.

The extended Newmark's method was validated for a case of strong ground motions. The permanent displacement of the block obtained by using this method was 14.5% lower than the recorded value (for the average value of the friction coefficient). The accuracy of the extended Newmark's method for complex signals is less than that stated for cyclic loading. Therefore, when assessing the slope stability, it is advisable to treat the material properties as a random variable.

The experimental results also show that the block acceleration is not constant during the phase of relative motion. Thus, the main assumption of the original Newmark's method is incorrect. Moreover, in the analysed cases, the original Newmark's method significantly underestimated the permanent displacement of the block.

The numerical analyses conducted by using the extended Newmark's method indicate that both the Arias Intensity and peak velocity of the excitation are good indicators of the impact of dynamic excitation on the dam's stability. The selection can be refined applying complementary information. In the case of Arias Intensity, it is the dominant frequency of the excitation, while in the case of peak velocity, it is the duration of the strong motion phase. It should be emphasized, that the directivity of the excitation has to be taken into account in the calculations.

References

Abrahamson, N.A. (2000), "State of the practice of seismic hazard evaluation", *ISRM International Symposium*, Melbourne, Australia, November.

Ambraseys, N.N., Smit, P., Douglas, J., Margaris, B., Sigbjornsson, R., Olafsson, S., Suhadolc, P. and Costa, G. (2004), "Internet site for European strong-motion data", *Bollettino di Geofisica Teoretica ed Applicata*, **45**(3), 113-129.

Aoi, Sh., Kunugi, T. and Fujiwara, H. (2004), "Strong-motion seismograph network operated by NIED: K-NET and KiK-net", *J. JPN Assoc. Earthq. Eng.*, **4**(3), 65-74. https://doi.org/10.5610/jaee.4.3_65.

Arias, A. (1970), "A measure of earthquake intensity", Massachusetts Inst. of Tech., Cambridge Univ. of Chile, Santiago de Chile.

Bolt, B.A. (1969), "Duration of strong motion", *Proceedings of 4th World Conference on Earthquake Engineering*, Santiago, Chile, January.

Bommer, J.J. and Acevedo, A.B. (2004), "The use of real earthquake accelerograms as input to dynamic analysis", *J Earthq. Eng.*, **8**(1), 41-91. https://doi.org/10.1080/13632460409350521.

Boore, D.M. (2005), "On pads and filters: Processing strong-motion data", *Bull. Seismol. Soc. Am.*, **95**(2), 745-750. http://doi.org/10.1785/0120040160.

Boore, D.M. and Bommer, J.J. (2005), "Processing of strong-motion accelerograms: Needs, options and consequences", *Soil Dyn. Earthq. Eng.*, **25**, 93-115. https://doi.org/10.1016/j.soildyn.2004.10.007.

Bradley, B.A. (2015), "Correlation of Arias intensity with amplitude, duration and cumulative intensity measures", *Soil Dyn. Earthq. Eng.*, **78**, 89-98. https://doi.org/10.1016/j.soildyn.2015.07.009.

Burkacki, D. and Jankowski, R. (2019), "Experimental study on models of cylindrical steel tanks under mining tremors and moderate earthquakes", *Earthq. Struct.*, **17**(2), 175-189. https://doi.org/10.12989/eas.2019.17.2.175.

Burkacki, D., Wójcik, M. and Jankowski, R. (2020), „Numerical investigation on behaviour of cylindrical steel tanks during mining tremors and moderate earthquakes", *Earthq. Struct.*, **18**(1), 97-111. https://doi.org/10.12989/eas.2020.18.1.097.

Chiou, B., Darragh, R.B., Gregor, N. and Silva, W. (2008), "NGA project strong-motion database", *Earthq. Spectra*, **24**(1), 23-44. https://doi.org/10.1193/1.2894831.

Chousianitis, K., Del Gaudio, V., Kalogeras, I. and Ganas, A. (2014), "Predictive model of Arias intensity and Newmark displacement forregional scale evaluation of earthquake-induced landslide hazardin Greece", *Soil Dyn. Earthq. Eng.*, **65**, 11-29. https://doi.org/10.1016/j.soildyn.2014.05.009.

Czerwionka, L. and Tatara, T. (2007), "Standard response spectra from chosen mining regions at Upper Silesian Coalfield", *Czasopismo Techniczne*, **2-B**/**2007**, 11-18. (in Polish)

Day, R.T. (2002), *Geotechnical Earthquake Engineering Handbook*, McGraw-Hill.

ESD (2015), European Strong-Motion Database, http://www.isesd.hi.is

Eurocode 8 (2004), Design of Structures for Earthquake Resistance, Part 1 and Part 5, European Committee for Standardization, Brussels, Belgium.

Falborski, T. and Jankowski, R. (2017), "Experimental study on effectiveness of a prototype seismic isolation system made of polymeric bearings", *Appl. Sci.*, **7**(8), 808. https://doi.org/10.3390/app7080808.

Falborski, T. and Jankowski, R. (2018), "Advanced hysteretic model of a prototype seismic isolation system made of polymeric bearings", *Appl. Sci.*, **8**(3), 400. https://doi.org/10.3390/app8030400.

Garini, E., Gazetas, G. and Anastasopoulos, I. (2011), "'Asymmetric Newmark' sliding caused by motions containing severe 'directivity' and 'fling' pulses", *Geotechnique*, **61**(9), 733-756. https://doi.org/10.1680/geot.9.P.070.

Gazetas, G. and Dakoulas, P. (1992), "Seismic analysis and design

of rockfill dams: State-of-the-art", *Soil Dyn. Earthq. Eng.*, **11**, 27-61. https://doi.org/10.1016/0267-7261(92)90024-8.

Grünthal, G. (1999), "Seismic hazard assessment for Central, North and Northwest Europe: GSHP Region 3", *Annali Di Geofisica*, **42**(6), 999-1011. https://doi.org/10.4401/ag-3783.

GSHAP (2015), Global Seismic Hazard Assessment Program, http://www.seismo.ethz.ch/static/gshap/ceurope/.

Haselton, C.B. (2009), "Evaluation of ground motion and modification methods: Predicting median interstory drift response of buildings", *PEER Ground Motion Selection and Modification Working Group*.

ICOLD (2016), "Selecting seismic parameters for large dams", Guidelines, Bulletin, **148**.

Jayaram, N., Lin, T. and Baker, J.W. (2011), "A computationally efficient ground-motion selection algorithm for matching a target response spectrum mean and variance", *Earthq Spectra*, **27**(3), 797-815. https://doi.org/10.1193/1.3608002.

Jibson, R.W. (1994), "Predicting earthquake-induced landslide displacements using Newmark's sliding block analysis", *Tran. Res. Rec.*, **1411**, 9-17.

Jibson, R.W. (2007), "Regression models for estimating coseismic landslide displacement", *Eng. Geol.*, **91**, 209-218. https://doi.org/10.1016/j.enggeo.2007.01.013.

Jibson, R.W. (2011), "Methods for assessing the stability of slopes during earthquakes-A retrospective", *Eng. Geol.*, **122**, 43-50. https://doi.org/10.1016/j.enggeo.2010.09.017.

Katsanos, E.I., Sextos, A.G. and Manolis, G.D. (2010), "Selection of earthquake ground motion records: A state-of-the-art review froma structural engineering perspective", *Soil Dyn. Earthq. Eng.*, **30**, 157-169. https://doi.org/10.1016/j.soildyn.2009.10.005.

Kaveh, A. and Mahdavi, V.R. (2017), "Modification of ground motions using wavelet transform and VPS algorithm", *Earthq. Struct.*, **12**(4), 389-395. https://doi.org/10.12989/eas.2017.12.4.389.

Korzec, A. (2016), "Effect of the vertical seismic accelerations on the stability of earth dams", *Arch. Hydro-Eng. Environ. Mech.*, **63**(2-3), 101-120. https://doi.org/10.1515/heem-2016-0007.

Korzec, A. (2021), "Extended Newmark method to assess stability of slope under bidirectional seismic loading", *Soil Dyn. Earthq. Eng.*, **143**, 106600. https://doi.org/10.1016/j.soildyn.2021.106600.

Korzec, A. and Jankowski, R. (2018), "Experimental study of the effect of vertical acceleration component on the slope stability", *J. Measure. Eng.*, **6**(4), 240-249. https://doi.org/10.21595/jme.2018.20420.

Kramer, S.L. (1996), *Geotechnical Earthquake Engineering*, Prentice-Hall Inc.

Lanzo, G., Pagliaroli, A. and Scasserra, G. (2015), "Selection of ground motion time histories for the nonlinear analysis of earth dams", *Proceedings of the XVI ECSMGE. Geotechnical Engineering for Infrastructure and Development*, Edinburgh, Scotland, September.

Lowrie, W. (2007), *Fundamentals of Geophysics*, Cambridge University Press.

Massa, M., Pacor, F., Luzi, L., Bindi, D., Milana, G., Sabetta, F., Gorini, A. and Marcucci, S. (2010), "The Italian ACelerometric Archive (ITACA): Processing of strong-motion data", *Bull. Earthq. Eng.*, **8**, 1175-1187. https://doi.org/10.1007/s10518-009-9152-3.

McGuire, R.K. (2001), "Deterministic vs. probabilistic earthquake hazard and risks", *Soil Dyn. Earthq. Eng.*, **21**, 377-384. https://doi.org/10.1016/S0267-7261(01)00019-7.

Mirek, J. and Lasocki, S. (2001), "SEJS-NET: extensive seismometric measurement system", *Proceedings of Natural Hazards in Mining*, Wieliczka, Poland, May. (in Polish)

Neethu, B., Das, D. and Garia, S. (2017), "Effects of ground motion frequency content on performance of isolated bridges with SSI", *Earthq. Struct.*, **13**(4), 353-363. https://doi.org/10.12989/eas.2017.13.4.353.

Newmark, N.M. (1965), "Effects of earthquakes on dams and embankments", *Geotechnique*, **15**(2), 139-160. https://doi.org/10.1680/geot.1965.15.2.139.

PEER (2015), The Pacific Earthquake Engineering Research Center, https://ngawest2.berkeley.edu/.

Pejovic, J.R., Serdar, N.N. and Pejovic R.R. (2017), "Optimal intensity measures for probabilistic seismic demand models of RC high-rise buildings", *Earthq. Struct.*, **13**(3), 221-230. https://doi.org/10.12989/eas.2017.13.3.221.

Romeo, R. (2000), "Seismically induced landslide displacements: a predictive model", *Eng. Geol.*, **58**, 337-351. https://doi.org/10.1016/S0013-7952(00)00042-9.

Romeo, R. and Prestininzi, A. (2000), "Probabilistic versus deterministic hazard analysis: an integrated approach for siting problems", *Soil Dyn. Earthq. Eng.*, **20**, 75-84. https://doi.org/10.1016/S0267-7261(00)00039-7.

Sarma, S.K. and Kourkoulis, R. (2004), "Investigation into the prediction of sliding block displacements in seismic analysis of earth dams", *Proceedings of 13th World Conference of Earthquake Engineering*, Vancouver, Canada, August.

Sawicki, A. and Chybicki, W. (2005), "Horizontal motion of a rigid block resting on accelerating subsoil", *Arch. Hydro-Eng. Environ. Mech.*, **52**(2), 147-160.

Sica, S., Santucci de Magistris, F. and Vinale, F. (2002), "Seismic behavior of geotechnical structures", *Ann. Geophys.*, **45**(6), 799-815. https://doi.org/10.4401/ag-3539.

Srbulov, M. (2008), *Geotechnical Earthquake Engineering. Simplified Analyses with Case Studies and Examples*, Springer.

Travasarou, T. (2003), "Optimal ground motion intensity measures for probabilistic assessment of seismic slope displacements", Ph.D. Dissertation, Civil and Environmental Engineering, University of California, Berkeley.

Trifunac, M.D. and Brady, A.G. (1975), "A study on the duration of strong earthquake ground motion", *Bull. Seismol. Soc. Am.*, **65**(3), 581-626. https://doi.org/10.1785/BSSA0650030581.

Trifunac, M.D. (1971), "Zero baseline correction of strong-motion accelerograms", *Bull. Seismol. Soc. Am.*, **61**(5), 1201-1211. https://doi.org/10.1785/BSSA0610051201.

Tsinidis, G., Di Sarno, L., Anastasios Sextos, A. and Furtner, P. (2020), "Optimal intensity measures for the structural assessment of buried steel natural gas pipelines due to seismically-induced axial compression at geotechnical discontinuities", *Soil Dyn. Earthq. Eng.*, **131**, 106030. https://doi.org/10.1016/j.soildyn.2019.106030.

Yang, J., Li, J.B. and Lin, G. (2006), "A simple approach to integration of acceleration data for dynamic soil-structure interaction analysis", *Soil Dyn. Earthq. Eng.*, **26**, 725-734. https://doi.org/10.1016/j.soildyn.2005.12.011.

Zembaty, Z. (2004), "Rockburst induced ground motion-A comparative study", *Soil Dyn. Earthq. Eng.*, **24**, 11-23. https://doi.org/10.1016/j.soildyn.2003.10.001.

DK